ACS NANO

www.acsnano.org

ARTICLE

A Spin-Dependent Model for Multi-Heme Bacterial Nanowires

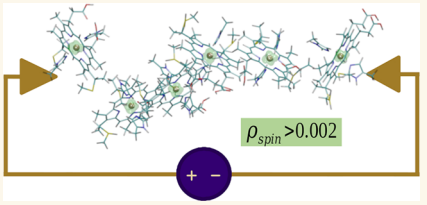
William Livernois* and M. P. Anantram

Cite This: *ACS Nano* 2023, 17, 9059–9068

Read Online

ACCESS | Metrics & More | Article Recommendations | Supporting Information

ABSTRACT: The electrical properties of conductive heme-based nanowires found in *Geobacter sulfurreducens* bacteria were investigated using spin-dependent density functional theory (DFT). Molecular orbitals were generated using a restricted open-shell model which was solved by applying constraints to the spin-separated unrestricted open-shell model. Charge transport was simulated at different length scales ranging from individual heme sites up to the monomer unit of the nanowire, looking at hopping and tunneling between neighboring heme porphyrins with different Fe oxidation states. The resulting spin-dependent DFT results indicate that tunneling rates between heme sites are highly dependent on oxidation state and transport pathway modeled. The model demonstrates the importance of spin dependence for electron hopping, oxidation state, and decoherence transport in cytochromes. Applying non-equilibrium's Green's function to the system confirmed a substantial decrease in decoherent charge transport for the oxidized molecule at lower Fermi energies. In addition, partial or full oxidation of the heme sites in the nanowire created conditions for spin-dependent transport that can be exploited for spin-filtering effects in nanodevices.



KEYWORDS: *density functional theory, bioelectronics, nanodevices, quantum transport, spin polarization*

Downloaded via UNIV OF WASHINGTON on July 21, 2023 at 23:32:28 (UTC).
See https://pubs.acs.org/sharingguidelines for options on how to legitimately share published articles.

Modeling mechanisms for charge transport in naturally occurring biological molecules can shed light on integration of these structures into nanoelectronics and biosensors. While many biological processes that involve charge transport are relatively slow compared to the requirements for modern electronics, limited by ion diffusion and chemical reactions, the *Geobacter sulfurreducens* bacteria has been researched extensively due the uniquely high conductivity of the OmcS cytochrome. This bacteria has been explored for a variety of electronics applications, taking advantage of the electron transfer mechanisms to generate electricity following the seminal work from the Lovely group.[1] Within the *G. sulfurreducens* bacteria charge transport has been demonstrated to occur primarily through the OmcS protein,[2] a cytochrome that consists of heme porphyrins stacked with alternating orientations along a helix protein scaffold as shown in Figure 1. The family of multiheme cytochromes have long been studied in the context of cellular redox chemistry, the OmcS protein is of particular interest due to its involvement in extracellular electron transport, participating in long-range charge transport with length scales on the order of microns.[3] Looking at the overall electronic structure and theoretical conductivities of the OmcS protein can help explain this behavior and elucidate further properties to explore in future devices.

Numerous previous studies have modeled charge transport in cytochromes using Marcus theory,[4−6] a semiclassical electron hopping model that uses tunneling magnitude and reorganization energy to determine the kinetics of electron transfer.[7] Using this method, each heme site is modeled in its donor or acceptor state, calculating rate constants that can be solved as a system of equations to determine the current. Density functional theory (DFT) methods can be combined with other empirical methods to generate the local orbitals on each donor and acceptor site using the electronic coupling between sites to calculate a hopping rate. Other works have applied quantum transmission models to cytochrome systems, looking at ballistic (purely coherent) transport[8] and mixed coherent and incoherent (hopping) transport.[9,10] While the high conductivity of the OmcS protein may suggest a faster transport method like ballistic transport, the high fluctuations of the biomolecule seem to suggest loss of coherence over the length scales. Despite studies showing that dephasing times in cytochrome systems can approach one picosecond,[11] this corresponds to the same time scale of an electron transfer between two hemes, and therefore loss of coherence is expected even at the heme to heme hopping length scale. While several multistep hopping models were initially

Received: December 3, 2022
Accepted: April 27, 2023
Published: May 3, 2023



© 2023 American Chemical Society

https://doi.org/10.1021/acsnano.2c12027
ACS Nano 2023, 17, 9059−9068

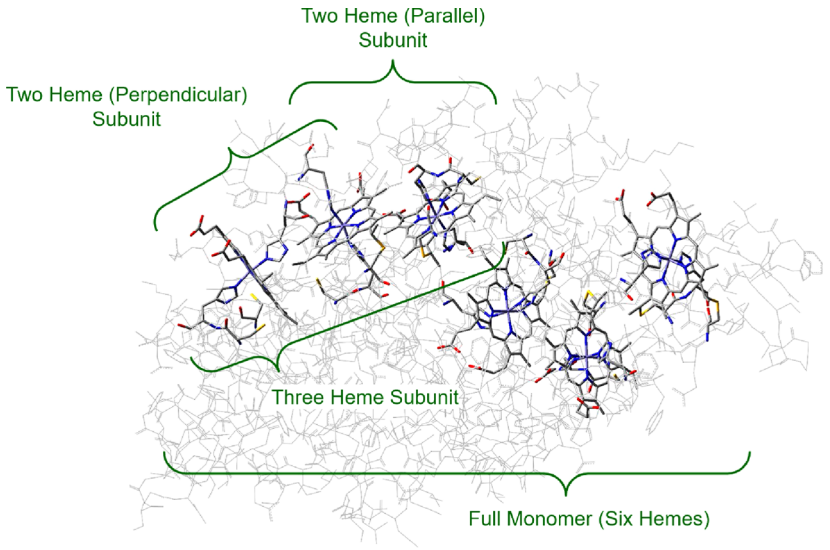


Figure 1. Structure of the OmcS protein highlighting the location of the heme porphyrin sites as well as the various sections used in this study.

considered for this work, the energy barrier for single step electron hopping was found to be much lower than the energy barrier of intermediate reactions. In this work we explored previously studied single step incoherent hopping models, where electron transfer is limited to onsite hopping kinetics, and compared them to decoherent quantum transport models that include multiple concurrent pathways of transport, including interaction with the environment. Using open-shell DFT methods, we were able to model the system in different oxidation states, predicting overall charge transport as well as spin-dependent transport along the cytochrome.

The OmcS nanowire was modeled with DFT at varying length scales to generate a system Hamiltonian, which acts as a single-electron operator used to construct molecular orbitals and determine electronic band structure. Using partitioning methods to create a local orbital basis at each heme site, hopping energies were calculated for the combined system looking at the impact of oxidation state, site conformation, and spin. As a final step, a decoherence model was applied to the system and Green's functions methods were used to measure overall quantum transmission. The non-equilibrium Green's function (NEGF) method was applied to the monomer unit of the cytochrome, where interactions with the electrodes and environment were represented by self-energy functions. Using this formalism, it is possible to determine the transmission spectrum and conductance of a two terminal nanodevice constructed from the cytochrome.

RESULTS AND DISCUSSION

For general DFT calculations it is most common to use the total energy of the many-electron system to calculate free energy differences for kinetics calculations as well as structure analysis. Marcus theory uses this total energy to calculate reorganization energy and free energy of oxidation while also using individual molecular orbitals to calculate the hopping energy between the donor and acceptor states. For the NEGF transmission calculations, a full single electron operator is needed to construct the Green's function and therefore it is necessary to look closely at the band structure of the system rather than a subset of orbitals. In the simplest case, all electrons are paired and electronic spin is not a variable in the calculation, referred to as the restricted closed shell case. For Hartree–Fock (HF) calculations, assuming a single Slater determinant for the multielectron wave function, the total energy for the restricted close shell case is given by

$$E = tr\hat{R}(2\hat{H} + 2\hat{J} - \hat{K}) \tag{1}$$

with the R matrix representing the occupancy of each orbital (one pair of electrons per orbital), the H matrix representing the one-electron core Hamiltonian, and the J and K matrices representing the Coulomb and exchange double electron integrals, respectively.[12] Note these electron integrals can be expanded to the DFT case by replacing the J and K matrices with the Coulomb and exchange-correlation operators that are density functionals. To get the single-electron operator one can apply the variational principle to get the Fock operator, given by

$$\hat{F} = \hat{H} + 2\hat{J} - \hat{K} \tag{2}$$

This operator can be diagonalized to give the single-electron energies of the system that obey Koopman's theorem, meaning that occupied energy levels correspond to ionization energies and unoccupied energy levels correspond to electron affinities.[13] For the cases of unpaired spin it is necessary to treat spins separately, where the unrestricted open-shell case is constructed by splitting the Fock operator into two arbitrary spin directions, labeled as alpha and beta spin. This gives us two Fock operators that in the HF formulation are written as

$$\begin{aligned} \hat{F}_\alpha &= \hat{H}_\alpha + \hat{J}_\alpha + \hat{J}_\beta - \hat{K}_\alpha \\ \hat{F}_\beta &= \hat{H}_\beta + \hat{J}_\alpha + \hat{J}_\beta - \hat{K}_\beta \end{aligned} \tag{3}$$

which resolves to eq 2 when the alpha and beta spins are equivalent. This formulation allows us to properly construct various spin states by modifying the number of alpha and beta electrons, whose total energy can be compared to determine the lowest energy spin configuration. However, these orbitals are not constrained to be eigenfunctions of the total spin operator, meaning that the spatial parts of alpha and beta orbitals may not completely overlap, due in part to the fact that density matrices are constructed for each spin independently.

https://doi.org/10.1021/acsnano.2c12027
ACS Nano 2023, 17, 9059–9068

Spin contamination arises from the loss of the total spin quantum number due to the mixing of alpha and beta spin states, with the specific formula given by

$$\delta_s = N_\beta - \sum_{i\in\alpha}\sum_{j\in\beta} |\langle i|j\rangle|^2 \tag{4}$$

In the limit of equal numbers of alpha and beta occupied states the self-consistent field (SCF) can converge to the RHF formulation, with alpha and beta orbitals matching exactly and therefore no spin contamination. Applying additional constraints to the orbital subspaces can ensure that the total spin quantum number is retained, which is the framework for the restricted open-shell model. In this formulation rather than separating the molecular orbitals into alpha and beta spin, they are separated into doubly occupied, partially occupied, and valence molecular orbitals.[14] Using operators for each shell, the equation for the total energy is given by

$$E = 2tr\hat{R}_c\left(\hat{H} + \hat{J}_c - \frac{1}{2}\hat{K}_c\right) + tr\hat{R}_o\left(\hat{H} + 2\hat{J}_c - \hat{K}_c + \frac{1}{2}\hat{J}_o - \frac{1}{2}\hat{K}_o\right) \tag{5}$$

which accounts for single electron energies as well as all interaction terms. Unique Fock matrices can be constructed for the closed, open, and valence shells with the following definitions

$$\hat{F}_c = \hat{H} + 2\hat{J}_c - \hat{K}_c + \hat{J}_o - \frac{1}{2}\hat{K}_o$$
$$\hat{F}_o = \hat{H} + 2\hat{J}_c - \hat{K}_c + \hat{J}_o - \hat{K}_o$$
$$\hat{F}_v = 2\hat{F}_c - \hat{F}_o = \hat{H} + 2\hat{J}_c - \hat{K}_c + \hat{J}_o \tag{6}$$

with the added constraint that doubly occupied orbitals (F_c) must be occupied before singly occupied (F_o) orbitals to generate the corresponding density matrices.[15]

From a quantum chemistry perspective, if we do not consider spin−orbit coupling or other relativistic terms then the spin quantum number must be retained, meaning that paired closed-shell electrons must be constrained to the same molecular orbital. While the restricted-open-formulation ensures this by partitioning orbitals by occupation, problems arise when attempting to generate unique molecular orbitals within each subspace. In the unrestricted case alpha and beta Fock operators can be treated completely independently for diagonalization, generating unique alpha and beta molecular orbitals to represent the occupied and valence states in the system. This means that it is trivial to form a single Hamiltonian operator combining both the alpha and beta Fock matrices to get

$$H_{\text{unrestricted}} = \begin{bmatrix} F_\alpha & 0 \\ 0 & F_\beta \end{bmatrix} \tag{7}$$

with off-diagonal terms set to zero signifying spin−spin and spin−orbit coupling are ignored. In the restricted open case, however, orbital occupation is interdependent between shells which leads to a more complicated formula for the combined Hamiltonian. This operator, called the unified coupling operator, can be formed with complementary-to-projection operators (ρ') assigning relative weights (given by variables a, b, and c) to each matrix to get

$$H_{\text{RO}} = a\rho_c' F_\beta \rho_c' + b\rho_o' F_\alpha \rho_o' + c\rho_v' F_v \rho_v' \tag{8}$$

where the subscripts "c", "o", and "v" refer to double-occupied, single-occupied, and valence shells and ρ_i' is the projection operator complementary to the shell i and is given by

$$\rho_i' = I - \rho_i \tag{9}$$

where I is the identity matrix.[16] The density matrices ρ_i represent the occupation within each of the subspaces of the three shells and sum up to unity. The weights a, b, and c represent a rotation between each of the subspaces to create a set of canonical orbitals, meaning that the total energy of the multielectron system remains constant. Therefore, the single electron energies can vary arbitrarily and, as a result, the unified coupling operator does not follow Koopman's theorem.

As an alternative approach the restricted open method can be written in terms of the unrestricted alpha and beta matrices, applying constraints to the orbitals to eliminate spin contamination while giving separate alpha and beta Fock matrices. These can be written as a function of the restricted open-shell doubly occupied and singly occupied Fock operators, with the transformation given by

$$F_\alpha = F_o$$
$$F_\beta = 2F_c - F_o \tag{10}$$

Because these matrices also satisfy the unrestricted open-shell eqs (eq 3), they form a set of unique orbitals whose eigenvalues satisfy Koopman's theorem.[17] In practice, due to the nature of the convergence criteria, the spin contamination of these orbitals is nonzero but greatly reduced from the unrestricted case, see part II of the Supporting Information (SI) for a side-by-side comparison between the models. The combined Hamiltonian can thus be created using eq 7 for quantum transmission calculations.

Spin-Separated Model Verification. As an initial study, the spin-separated Hamiltonian was constructed for both the free Fe ion and the smaller ferro/ferricyanide ($Fe(CN)_6$) systems. In the case of the free Fe ion, it was confirmed that high-spin states were preferred (spin splitting energies ranging from 3.5 to 8.0 eV for both oxidation states), although some of the d-orbital degeneracies were found split because of electron repulsion between occupied d-orbitals. Looking at the generated band structure we can see that the spin-separated HOMO energies line up closely with the experimentally determined ionization energies[18] while the combined Fock HOMO energies do not follow this trend (see Table S3 and Figure S1 in the SI). This confirms that the spin-separated model does follow Koopman's theorem.

As a second test the energy levels of the coordinated ferricyanide (oxidized state) and ferrocyanide (reduced state) ion were modeled using the spin-separated Hamiltonian. The ferro/ferricyanide system was chosen for comparison due to similarity with the heme system, which also has octahedral coordination with similarly spaced organic ligands (2−2.3 Å in the heme case vs 1.96 Å in the ferro/ferricyanide case). Upon coordination in the ferro/ferricyanide case, any d-orbital degeneracy was broken, and the low-spin state was found to be energetically preferred, as predicted by ligand field theory and confirmed by our DFT calculations. The resulting band diagrams (and spin-splitting energies) are shown in Figure 2, and the band gaps can be directly compared to absorption peaks that have been identified for each oxidation state, which

https://doi.org/10.1021/acsnano.2c12027
ACS Nano 2023, 17, 9059−9068

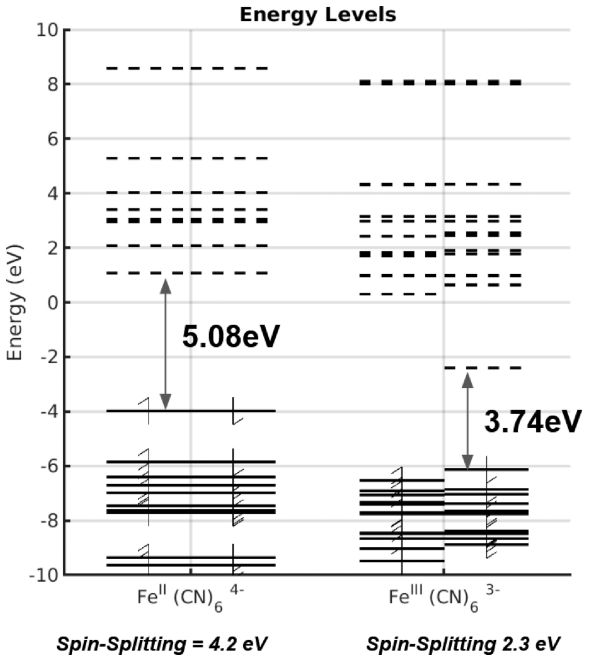
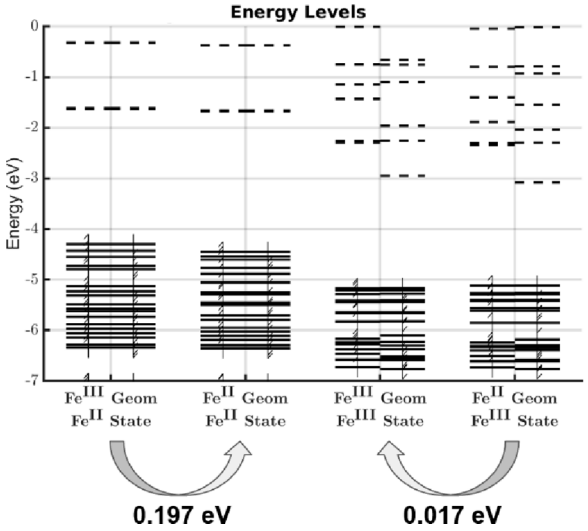


Figure 2. Energy level diagrams for ferrocyanide (left) and ferricyanide (right) showing the calculated band gaps and high-spin/low-spin splitting energies. The band gaps of 5.08 and 3.74 eV correspond to photon wavelengths of 243 and 330 nm, respectively.

are found at wavelengths ranges of 205−235 and 310−340 nm for the presence of ferrocyanide vs ferricyanide ions, respectively.[19] This result serves as experimental validation of the band gap calculated from the alpha and beta orbitals of the restricted open-shell approach and as further confirmation of spin separate treatment for transport modeling.

OmcS Nanowire Modeling. Ligand field theory has shown that while the uncoordinated heme prefers a high-spin state, axial histidine coordination on both sides of the heme shifts the point group from D4h to Oh and the ground state prefers the lower-spin state for both reduced and oxidized hemes. This was confirmed for the single hemes coordinated with histidines on both sides—the reduced Fe (II) system shows energetic preference to the singlet state and oxidized Fe (III) system shows energetic preference to the doublet state. High-spin ground states only occur with uncoordinated or single-sided coordinated hemes, as shown previously[20] and confirmed with our model. Orbitals were found to be more delocalized in the charged Fe(III) oxidation state, with the band gap lowering from 2.9 to 2.0 eV. An average reorganization energy of 0.11 eV was calculated between the two charge states on the deprotonated structure, with minimal band structure shift in either state, as shown in Figure 3. The reorganization energy was calculated using the total DFT energy difference between each geometry, as described in the Hopping Energy Calculations section of the Methods, with the details of further calculations included in the SI. To check the alignment of spin states, two-heme pairs were modeled in parallel and perpendicular configurations, and spin-splitting energies were calculated. In the two-heme case the low-spin ground state was confirmed for each individual heme and spin alignment was energetically favorable between heme sites both in the parallel and perpendicular conformations. This spin configuration was applied to all larger fragments as the ground state electronic structure. A full table of spin states calculated for each fragment, as well as the splitting energies and ground state DFT energies, are given in Table S1 in the SI.

Hopping energies were calculated for all four charge states of the three-heme subunit to compare all pathways of charge transfer between heme sites. The three-heme subunit was chosen as a model system because of the presence of both parallel and perpendicular conformations, allowing calculation of nearest neighbor hopping energies for all configurations. In addition, the four oxidation states represent four charge transfer methods: (a) fully reduced, HOMO−HOMO transitions, $Q = -6$; (b) hole transport, HOMO−LUMO transitions with oxidized central heme, $Q = +1$; (c) electron transport, HOMO−LUMO transitions with reduced central heme, $Q = +2$; and (d) fully oxidized, HOMO−HOMO transitions, $Q = +3$. This means that case (b) was calculated as electron transfer from the outer hemes to the central heme and



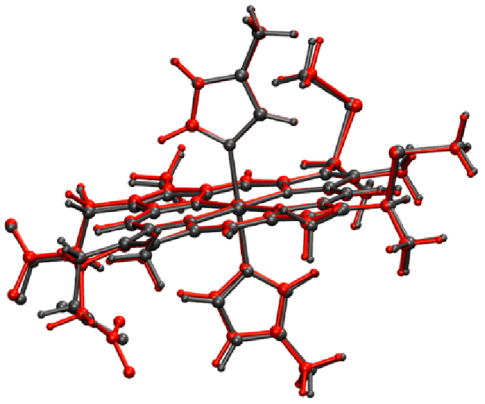


Figure 3. Reorganization impact on the deprotonated heme structure, showing the shift in band structure during reorganization on the left and the physical coordinate changes in the right, where the red structure is in the oxidized state and the gray structure is in the reduced state. DFT energy differences are calculated between geometries at the same oxidation state.

https://doi.org/10.1021/acsnano.2c12027
ACS Nano 2023, 17, 9059−9068

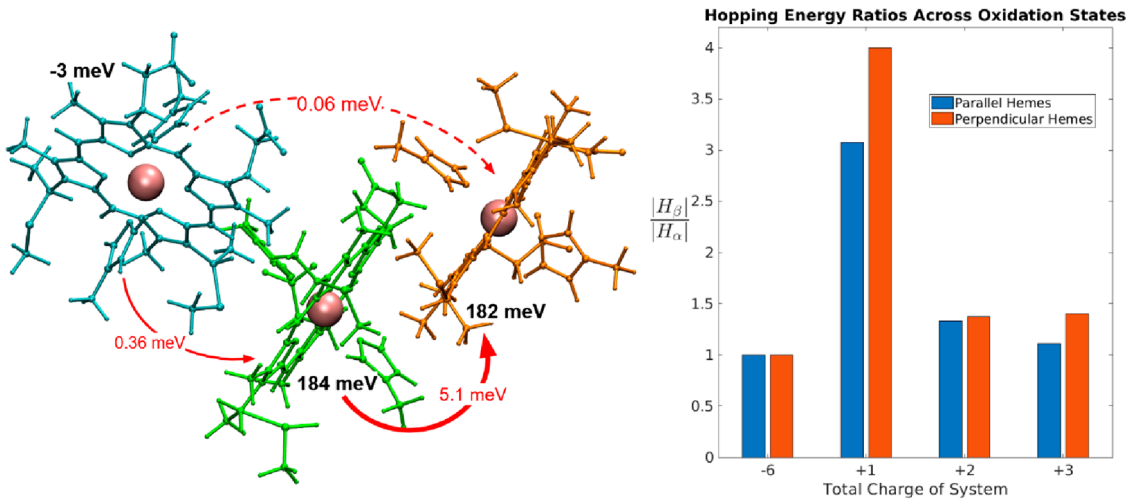


Figure 4. Modeling results from the three-heme subunit showing the onsite energies relative to the HOMO and hopping energies for the reduced case ($Q = -6$ corresponding to 6 COO^- groups) on the left and the spin dependence of hopping energies, plotted as a ratio of the α and β hopping energies, on the right. The values of the hopping energies for each oxidation state are given in Table S7 in the SI, with the transfer pathway for each hopping energy given in Figure S4.

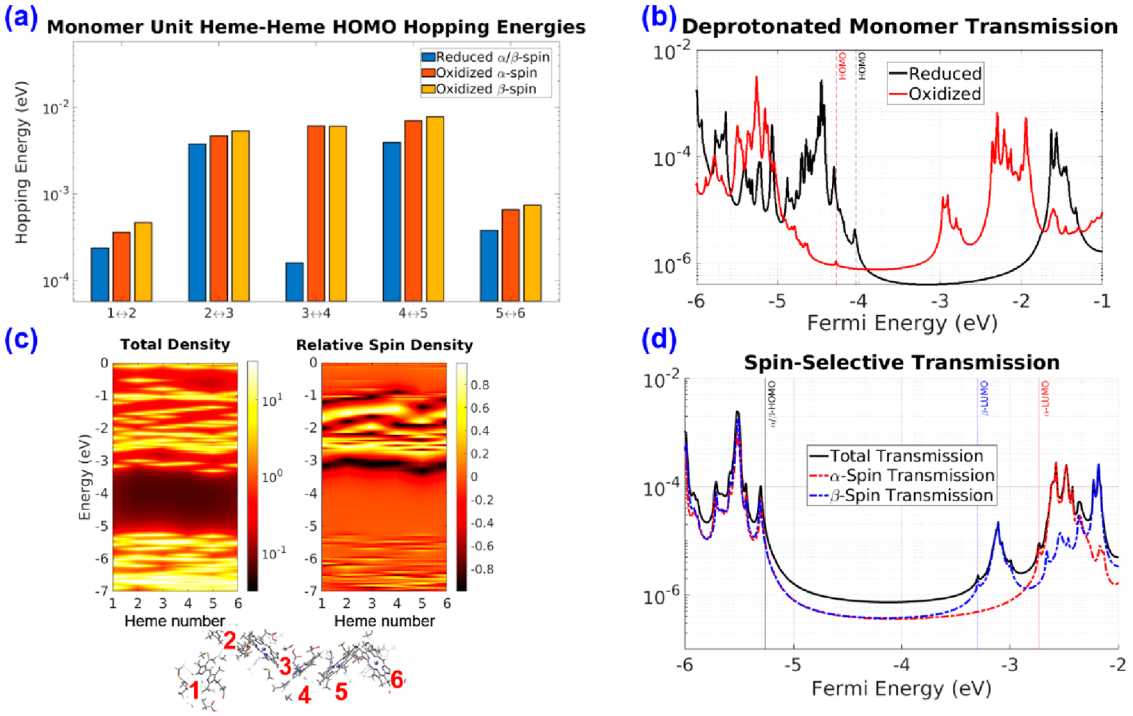


Figure 5. Electron transport across the six heme monomer unit with (a) comparison of HOMO−HOMO hopping energies for the fully oxidized and fully reduced cases, (b) comparison of quantum transmission of the nanowire in the deprotonated (COO^-) oxidized and reduced cases, (c) total density of states across the fully oxidized monomer, segmented by hemes labeled in the diagram, as well as the relative spin density, given by $(\rho_\alpha - \rho_\beta)/\rho_{tot}$, and (d) spin dependency of transmission for the fully oxidized monomer.

case (c) was calculated as electron transfer from the central heme to the outer hemes. The terminology and methods for each of these calculations is discussed in the SI with the accompanying visualization in Figure S4. We determined the hopping energies between perpendicular hemes were an order of magnitude smaller than parallel hemes for all cases, matching up with previous calculations[21] as depicted in Figure 4. The hopping energies for the oxidized case have a significant spin dependency, resulting from the spin alignment between the hemes discussed earlier. The ratios of the alpha and beta charge transfer energies were plotted in the right plot of Figure 4, showing the spin dependency especially in the $Q = +1$ hole-transfer case favoring the beta (valence) spin state.

As a final step, the model was applied to full monomer unit to generate a system Hamiltonian that can be used for hopping and decoherent models. For this six-heme system, four cases were modeled: reduced Fe^{II} vs oxidized Fe^{III} and deprotonated COO^- vs protonated COOH on the propionate groups. An analysis of incoherent hoping was conducted on the fully reduced (Fe^{II} and COO^-) and the fully oxidized (Fe^{III} and COOH) states, with HOMO−HOMO hopping energies plotted in Figure 5a. These results show a drastic increase in

https://doi.org/10.1021/acsnano.2c12027
ACS Nano 2023, 17, 9059−9068

hopping energy for the oxidized case as well as some spin dependency. This is especially notable for the hopping energy between hemes 3 and 4, which have a perpendicular conformation, showing the importance of modeling electron delocalization across hemes in the nanowire. A fuller picture of electron transport was constructed by using Green's functions to model all orbital interactions. This was used to calculate local density of states for the fully oxidized case as a function of energy for each heme, looking at both the total electron density and spin density ratio as shown in Figure 5c. These plots show current pathways at Fermi energies near the HOMO and LUMO bands with high-spin polarization in the LUMO band. This was confirmed by plotting the spin-dependent transmission in Figure 5d, which shows up to 100× difference in decoherent transmission between alpha and beta spins at higher Fermi energies. The decoherent transmission was compared for the deprotonated COO^- cases as a function of Fermi Energy and plotted in Figure 5b to compare with experimental results at neutral pH. The calculated transmission at energies between −5 and −4.5 eV are significantly higher for the reduced case despite low HOMO−HOMO hopping energies, most likely related to the shift in HOMO energy between the oxidation states. In addition, the transmission at the HOMO energy for the reduced case is about 4× higher than for the oxidized case. Both observations from the decoherent model qualitatively match up with recent experimental results.[4] A separate calculation confirms that the shift in transmission curve is caused primarily by the change in oxidation state of the Fe center, with only a small contribution from reduction of the carboxylate groups on the heme, see Figure S6 in the SI for a direct comparison of the results for these four cases.

CONCLUSIONS

To understand electron transport in the OmcS heme nanowire structure we have applied ab initio methods to generate molecular orbitals of the full system. This allows us to consider all mechanisms of charge transfer across the protein, rather than applying constraints to specific donor and acceptor sites. Hopping energy calculations did not include any kind of nuclear coordinate shift, although reorganization was found to not significantly affect the orbital energies for the single heme case. Although the hopping energy between heme sites in the cytochrome is smaller than those of other biological systems, like DNA, we have shown that orbital delocalization plays a key role in transport, with band formation in the oxidized state creating a significant increase in tunneling rates near the HOMO energy. The open-shell methods used to generate a spin-separated Hamiltonian can be applied to any system to develop an electron transport model, especially when considering interactions between many orbitals. While unrestricted models are computationally efficient and tend to be more accurate for determining ground state energies due to fewer constraints on the system, the resulting molecular orbitals can break spin symmetry. We propose using the restricted open model to generate the Hamiltonian and include multiple concurrent pathways across multiple oxidation states as well as spin-dependent electron transport. We also found that the implementation of the restricted open-shell solver greatly reduced the spin contamination for all cases (see Table S5 of the SI) and shifted the size and magnitude of the transmission peaks (see Figure S3 of the SI). Green's function methods allow us to include all interactions of orbitals for modeling electron transport and consider a mix of different charge states. We were able to use the NEGF formulation to model transport across different oxidation states and confirm the experimental results, which show that the oxidation of the OmcS reduces conductivity. While hopping energies between neighboring sites were calculated to be higher in the fully oxidized case, the overall transmission is higher for the reduced case at lower Fermi energies, which can be attributed to the overall shift in orbital energies.

Our decoherent transport model does not explicitly include reorganization or any nuclear coordinate shift, an assumption supported by the single heme reorganization calculations. Instead, energy fluctuations caused by interactions with the environment were accounted for by the decoherence probes applied using a model that has been developed in previous works.[22,23] Even to include nonadiabatic effects like reorganization energy there are several intermediate steps that must be accounted for besides the total shift in energy of the system. Marcus theory does not consider the full pathway of charge transfer between the donor and acceptor, which includes a shift in energy between donor and acceptor orbitals as well as charging effects that occur during the transition. Looking at the case of the single coordinated heme site there is a local charging and discharging energy from the polarization of orbitals during charge transfer, which can be calculated by looking at the shift in energies of the LUMO orbital as it becomes occupied.[24] We have determined these energies to be significant (0.6−0.7 eV for each heme site) when compared to the total free energy of oxidation (3.7−4.2 eV for each heme site, see Table S4 in SI). To include such effects in the model, we propose using a self-consistent NEGF formulation and look at wave function dynamics during electron transfer. This would need to be accomplished on a smaller scale model, as the computation costs of such a calculation requires numerous DFT calculations to converge the electron density at each time step.

The consideration of spin was crucial for modeling oxidation states because removal of an electron from a pair inherently generates spin. This is especially true for an organometallic system like heme where the Fe center can exist in several stable oxidation states. By applying a collinear spin model, we have shown the impact spin can have on electron transport in the system even with higher order effects ignored. While these effects would not significantly contribute to the Hamiltonian due to the low electron transmission rates and low atomic weight of all atoms, this model does not account for effects like spin−orbit coupling as well as other spin-dependent effects like chiral-induced spin selectivity, partial orbital occupation from self-consistent calculations, and spin transitions caused by decoherence. Our results demonstrate significant spin-dependent transport, especially in the valence band, and we suspect that considering these higher-order effects will accentuate these spin-dependent effects.

We suggest further experiments to measure the spin dependence of electron transport, especially to develop spintronics based on these protein nanowires. Our models consider ambient conditions, both with the choice to model with an implicit solvent model as well as the temperature of 300 K used to determine the orbital occupation (any degeneracies caused by thermal energy). Therefore, we would recommend an experimental setup in these conditions using ferromagnetic contacts that would allow one to polarize the electron spin entering the cytochrome to measure

https://doi.org/10.1021/acsnano.2c12027
ACS Nano 2023, 17, 9059−9068

magnetoresistance. Such a setup would be similar to that of Xiong et al. that was used to look at spin filtering in organic materials.[25] Measuring the magnetoresistance and hysteresis effects in this system is paramount to incorporation in future nanodevices.

METHODS

Ab Initio DFT Modeling. All DFT calculations were done using Gaussian-type orbitals and the Gaussian 16 software package.[26] The B3LYP functional was used with the restricted closed shell model used for singlet states and the restricted open-shell model used for states with net spin (nonsinglet states). An exception was the free Fe ion case where HF was used. To determine the ground state spin (and subsequent spin state splitting energies) we used the unrestricted solver result as a guess for the restricted open model to increase the accuracy of the total energy with the added spin constraints.[27] The ground spin state was calculated by comparing the DFT energies of multiple spin multiplicities for the same coordinates and choosing the lowest energy case. To ensure consistency in the calculated ground spin state, DFT energies were compared within the unrestricted and restricted open models, and no discrepancies were found. The Hamiltonian was constructed based on the formula from eq 7 using the resulting alpha and beta Fock matrices from the restricted open-shell calculation rather than the unified coupling operator matrix. A mixed orbital basis was used: the LANL2DZ basis with the effective core potential[28] for Fe atoms in the heme center and the 6-31G** Pope basis set[29] for all other atoms. The one exception to this basis set choice was the reorganization energy calculations, which used the 6-31G++** Pope basis set with added diffuse orbitals to improve calculation accuracy. To account for water solvent effect, the polarizable continuum model (PCM) was applied to account for the dielectric behavior of the aqueous environment.[30]

The free Fe ion was the only system modeled using the restricted open Hartree−Fock (ROHF) method to force the full weight of the exchange term for the single atom. Spin-splitting energies were calculated by taking the difference in energies of each possible spin multiplicity based on 3d and 4s orbital occupation. The ferro/ferricyanide system was constructed with a starting set of coordinates that were optimized by minimizing DFT energy for both oxidation states in their ground state spin configuration.

The OmcS nanowire structure was modeled in sections ranging from one heme center to the full six heme monomer using beta-carbon terminated histidine and cysteine functional groups. This method was developed in a previous work[21] based on the observation of minimal interaction with surrounding protein[6] and confirmed with DFT results showing the impact of backbone interactions on the band structure. Using the structures from this work (with initial coordinates from PDB ID 6EF8[3]) multiple oxidation states were compared, with the ground state spin multiplicity confirmed across spin multiplicities for fixed atomic coordinates. Atomic coordinates were given for the fully reduced and fully oxidized single heme structure after energy minimization in Table S2 in the SI, all other structures used can be easily calculated from the PDB structure in ref 3. Spin alignments between heme sites were modeled by setting an initial spin constraint for each fragment and comparing the total energy of the converged SCF. For all cases, the fully reduced (Fe^{II}) state the hemes were modeled in their deprotonated state while all other partial and fully oxidized (Fe^{III}) states were modeled with fully protonated hemes. Comparing energies of the isoelectronic single heme structures showed an energy difference between the protonated and deprotonated structures that was +25 eV for the reduced state and +26 eV for the oxidized state. Since the ionization energy of a hydrogen atom is 13.6 eV, this matches up with the approximate energy of removing two hydrogens, with the oxidized state having a slightly higher energy barrier for hydrogen removal. Additional calculations for the monomer unit were conducted with the deprotonated Fe^{III} state and protonated Fe^{II} state to look at the effect of protonation on transport. The protonation and oxidation states for each structure modeled are included in Table S1 in the SI.

All structures were calculated using the default solvers and "tight" convergence criteria of the Gaussian 16 software package with one exception: the oxidized deprotonated monomer unit. The default "tight" convergence criteria stop the SCF cycle after calculating an RMS change in the density matrix below 10^{-8} and a maximum change in the density matrix below 10^{-6}. For the oxidized deprotonated monomer unit, this convergence criteria were loosened to an RMS change in the density matrix below 10^{-6} and a maximum change in the density matrix below 10^{-4}. In addition, the unrestricted open-shell B3LYP wave function, used as a guess for the restricted open solver, kept the "tight" convergence criteria but required using the quadratic convergence SCF implementation to converge. Convergence of the SCF was not possible without these modifications, but despite this looser convergence criteria the spin contamination of the unrestricted B3LYP wave function was reduced from 0.23 to 0.02 for this case.

Hopping Energy Calculations. We compare our hopping, reorganization, and ionization energies to those previously calculated in ref 4. The single heme case was modeled with full DFT optimization to determine a reorganization energy and quantify the impact of reorganization on the band structure and determine free energy differences, both of which are exponential factors in the Marcus Theory rate calculation, given by

$$k_{et} = \frac{2\pi}{\hbar}|H_{ab}|^2 \frac{1}{\sqrt{4\pi\lambda k_B T}} \exp\left(-\frac{(\lambda + \Delta G_{ox})^2}{4\lambda k_B T}\right) \tag{11}$$

where λ is the reorganization energy, ΔG_{ox} is the free energy of oxidation, and H_{AB} is the hopping energy. Reorganization energy was calculated for four different cases of the single heme structure: protonated and deprotonated carboxylate groups (COOH vs COO^-, respectively) as well as constrained versus unconstrained coordinating atoms. Considering the protonation of the carboxylates allowed us to check the effect of the carboxylate oxidation state on the reorganization, looking only at the reorganization caused by the Fe redox reaction decoupled from the effects of reorganization due to protonation or deprotonation that may occur by varying pH. While the effects of the backbone on reorganization were not directly considered, the constraints placed on the coordinating hemes allowed us to look at the limiting cases of the force constraints on the coordinating heme groups. Freezing the central iron atom and six coordinating nitrogen atoms looks at the limit where the backbone is completely rigid, while eliminating the constraints looks at the limit where the groups have no applied force from the backbone. The reorganization energies were calculated by running a full DFT optimization applied to the four structures (with or without the constraints) in the two oxidation states and comparing the energy differences. Energy band diagrams and a visualization of the coordinate shifts are given for each case in Figure S2 in the SI with DFT energies and reorganization energies reported in Table S4. This reorganization energy was calculated as a difference in total DFT energy between both optimized geometries, averaging the energy difference between geometries in the oxidized electronic state and the geometries in the reduced electronic state. We have reported the reorganization energy calculated for the unconstrained and deprotonated case in Figure 3, which most closely matches the calculations previously done in the literature, with the computed reorganization energy of 0.11 eV. This is almost an order of magnitude lower than the previously reported values of 0.7−1.2 eV.[4] Though our reorganization energy does not account for the atomic shifts of the backbone and coupling with neighboring hemes, which would explain some of the numerical difference in our answer, the resulting band structures before and after reorganization show minimal orbital energy shift in all cases, indicating reorganization does not significantly affect the electronic structure of the heme unit.

Hopping energies between nearest neighbor heme groups were calculated using the three- and six-heme subunits, using the similar approach by Breuer et al.[6] to take the RMS of the couplings extracted from a block diagonal Hamiltonian. In this setup, the onsite orbitals are represented by the HOMO or LUMO orbitals of the heme site, and the couplings between these orbitals (off-diagonal terms in the

https://doi.org/10.1021/acsnano.2c12027
ACS Nano 2023, 17, 9059−9068

Hamiltonian) are averaged to generate a hopping energy (H_{AB}). In our implementation the DFT calculations were applied to the fully interacting multiheme system, which allowed us to use linear transformations to partition the Hamiltonian by heme site and extract off-diagonal orbital couplings. This was done by diagonalizing the separated blocks of the Hamiltonian and constructing a transformation matrix for the combined Hamiltonian given by

$$V = \begin{bmatrix} V_1 & \cdots & 0 \\ \vdots & \ddots & \vdots \\ 0 & \cdots & V_i \end{bmatrix} \tag{12}$$

where V_i is a square matrix of eigenvectors for block i and V is a block diagonal matrix. The transformed Hamiltonian is given by

$$H' = V^{\dagger}HV \tag{13}$$

where rows and columns represent the local molecular orbitals for each block and off-diagonal terms represent electronic couplings between molecular orbitals. Hopping energies were calculated by analyzing electronic couplings from the HOMO band of the donor fragment to thermodynamically available orbitals ($\Delta E \leq k_B T \approx 0.026$ eV) in the acceptor fragment at the edge of the band gap. For charge transfer between hemes of varying oxidation state, the charge transfer occurred from the HOMO band of the reduced heme complex to the LUMO orbital of the oxidized heme (there were not any thermally available LUMO orbitals where $|E_{LUMO} - E_{(LUMO+N)}| \leq k_B T$). As a comparison, charge transfer between hemes of the same oxidation state was calculated from the HOMO band of the donor heme to the HOMO band of the acceptor heme, including all thermally available HOMO orbitals ($|E_{HOMO} - E_{(HOMO-N)}| \leq k_B T$). Hopping energies were calculated between orbitals of the same spin (alpha or beta) except in the singlet case when alpha and beta orbitals were always found to be equivalent.

Green's Function Transport Calculations. The NEGF method was applied to the system Hamiltonian generated from the Fock and Overlap matrices using a Löwdin transformation to convert to an orthogonal atomic orbital basis set. The transmission spectrum was determined using the Green's function method, starting with the retarded Green's function given by

$$[EI - (H + \Sigma_L + \Sigma_R + \Sigma_B)]G^r = I \tag{14}$$

where E is the energy, H is the system Hamiltonian, $\sum_{L/R}$ is the left/right contact self-energy, and $\sum_B$ is the self-energy of the phase breaking decoherence probes that are used to model decoherence in the system.[22] For each of these self-energy matrices the wide-band limit approximation is used, which ignores the real part of the matrices and treats them as energy independent parameters defined at each atom at the contact.[31] The left and right contact energies are given by $\sum_{L/R} = \frac{-i\Gamma_{L/R}}{2}$ and the decoherence probe self-energies are defined similarly as $\sum_{B,n} = \frac{-i\Gamma_n}{2}$ for each of the n probes. The Green's function can be directly used to calculate the local density of states (DOS) at an energy, given by

$$\text{LDOS}\ (\psi_i, E) = -\frac{1}{\pi}\text{Im}[G^R(i, i, E)] \tag{15}$$

where ψ_i is the i-th basis orbital and $G^R(i,i,E)$ is the diagonal element of the Green's function at that energy. This can be used to look at local density of states for different fragments of the system, summing across orbitals in each molecule fragment. The diagonal components can be summed to give the total density of states as a function of energy:

$$\text{DOS}(E) = -\frac{1}{\pi}\mathbf{tr}[\text{Im}[G^R(E)]] \tag{16}$$

Rather than having discrete states, the broadening contribution from the contacts creates a continuous DOS spectrum across energies. A transmission spectrum can also be obtained from the Green's function, and we can define the transmission between probes n and m to be

$$T_{nm}(E) = \mathbf{tr}[\Gamma_n G^R(E)\Gamma_m[G^R(E)]^{\dagger}] \tag{17}$$

where probes n and m are inclusive of electrical contact or Büttiker probes. Plugging this into the Landauer equation gives a general equation for current through a given probe as

$$I_n = \frac{2q}{h}\sum_m \int T_{nm}(E)[f_n(E) - f_m(E)]\mathrm{d}E \tag{18}$$

where $f_n(E) = 1 + \exp\left(\frac{E - E_{f,n}}{K_B T}\right)$ is the Fermi distribution defined at probe n. Since the total current at each Büttiker probe is zero and current only flows between the left and right contacts, the transmission term can be simplified and combined to give

$$T_{\text{eff}} = T_{LR} + \Sigma_n\Sigma_m(T_{ln}W_{nm}^{-1}T_{mR}) \tag{19}$$

where n and m are summed over the decoherence probe sites and W_{nm}^{-1} is the inverse of $W_{nm} = (\sum_{n\neq l}T_{nl})\delta_{nm} - T_{nm}(1-\delta_{nm})$, an operator that propagates scattering at each probe site. Therefore, the first term in eq 19 defines the coherent transport while the second accounts for decoherence. From this transmission the zero-bias conductance is obtained by taking the derivative of eq 18 with respect to the chemical potential difference and plugging in eq 19 to get

$$G(E_f) = \frac{2q^2}{h}\int T_{\text{eff}}(E)\frac{\partial f(E - E_f)}{\partial E}\mathrm{d}E \tag{20}$$

which can be directly compared to experimental results. Note that in the low temperature limit the effective transmission is proportional to the zero-bias conductivity at that energy. For this study probe self-energies were applied based on previous work with other biomolecular systems ($\Gamma_{L/R}$ = 0.1 eV, Γ_B = 0.01 eV).[23] These self-energy values represent a high coupling with a metal contact on the left and right, making the molecule the bottleneck for charge transfer.

Transmission calculations were conducted for smaller sections of the OmcS monomer unit to look at transport at different length scales. Changing charge and spin state at each of these length scales impacted orbital location and energy caused by electron−electron repulsion. To model nonsinglet states (with unpaired spin states) the DFT functional used a restricted open-shell approach to generate the alpha and beta Fock matrices. The results for the minimum energy spin multiplicity were reported, and the full Hamiltonian was generated for transport calculations by separating the alpha and beta states. While the Green's function calculation used the combined Hamiltonian (from eq 7) to determine the total transmission, spin-dependent transport was measured by dividing the transmission matrix into quadrants.[32] Because spin−orbital coupling was not included in these calculations the off-diagonal terms (hopping parameters between alpha spin states and beta spin states) were set to zero leading to only two reported transmission values (alpha transmission and beta transmission) without cross terms.

ASSOCIATED CONTENT

Supporting Information

The Supporting Information is available free of charge at https://pubs.acs.org/doi/10.1021/acsnano.2c12027.

Heme nanowire spin state energies, Fe ionization energy comparison, reorganization energy calculations, spin contamination and constrained UHF formulation, hole/electron modeling in the three-heme subunit, monomer unit structure and contact sites, and monomer oxidation state transmission comparison. The corresponding data tables (Tables S1−S7) and figures (Figures S1−S6) are referenced throughout the main text to provide additional details and support for the claims of the paper (PDF)

https://doi.org/10.1021/acsnano.2c12027
ACS Nano 2023, 17, 9059−9068

AUTHOR INFORMATION

Corresponding Author

William Livernois − *Department of Electrical and Computer Engineering, University of Washington, Seattle, Washington 98195, United States;* orcid.org/0000-0001-8637-1213; Email: willll@uw.edu

Author

M. P. Anantram − *Department of Electrical and Computer Engineering, University of Washington, Seattle, Washington 98195, United States*

Complete contact information is available at: https://pubs.acs.org/10.1021/acsnano.2c12027

Author Contributions

The manuscript was written through contributions of all authors. All authors have given approval to the final version of the manuscript.

Funding

National Science Foundation Grant Numbers 1807391/1807555 (SemiSynBio Program) and FMSG - 2036865 (Future of Manufacturing) and National Defense Science and Engineering Graduate Fellowship.

Notes

The authors declare no competing financial interest.

ACKNOWLEDGMENTS

We would like to thank Professor Walid Hassan for his help understanding spin states of coordinated metals and Dr. Mike Frisch for his correspondence and help with Gaussian simulations. All simulations were conducted on the Hyak supercomputing cluster at the University of Washington.

ABBREVIATIONS

OmcS, outer membrane cytochrome S; HOMO, highest occupied molecular orbital; LUMO, lowest unoccupied molecular orbital; RMS, root mean square

REFERENCES

(1) Bond, D. R.; Lovley, D. R. Electricity Production by *Geobacter Sulfurreducens* Attached to Electrodes. *Appl. Environ. Microbiol.* **2003**, *69* (3), 1548−1555.

(2) Malvankar, N. S.; Vargas, M.; Nevin, K. P.; Franks, A. E.; Leang, C.; Kim, B. C.; Inoue, K.; Mester, T.; Covalla, S. F.; Johnson, J. P.; Rotello, V. M.; Tuominen, M. T.; Lovley, D. R. Tunable Metallic-like Conductivity in Microbial Nanowire Networks. *Nat. Nanotechnol* **2011**, *6* (9), 573−579.

(3) Wang, F.; Gu, Y.; O'Brien, J. P.; Yi, S. M.; Yalcin, S. E.; Srikanth, V.; Shen, C.; Vu, D.; Ing, N. L.; Hochbaum, A. I.; Egelman, E. H.; Malvankar, N. S. Structure of Microbial Nanowires Reveals Stacked Hemes That Transport Electrons over Micrometers. *Cell* **2019**, *177* (2), 361−369.e10.

(4) Dahl, P. J.; Yi, S. M.; Gu, Y.; Acharya, A.; Shipps, C.; Neu, J.; Patrick O'Brien, J.; Morzan, U. N.; Chaudhuri, S.; Guberman-Pfeffer, M. J.; Vu, D.; Yalcin, S. E.; Batista, V. S.; Malvankar, N. S. A 300-Fold Conductivity Increase in Microbial Cytochrome Nanowires Due to Temperature-Induced Restructuring of Hydrogen Bonding Networks. *Sci. Adv.* **2022**, *8* (19), 7193.

(5) Kaila, V. R. I.; Johansson, M. P.; Sundholm, D.; Wikström, M. Interheme Electron Tunneling in Cytochrome c Oxidase. *Proc. Natl. Acad. Sci. U. S. A.* **2010**, *107* (50), 21470−21475.

(6) Breuer, M.; Rosso, K. M.; Blumberger, J. Electron Flow in Multiheme Bacterial Cytochromes Is a Balancing Act between Heme Electronic Interaction and Redox Potentials. *Proc. Natl. Acad. Sci. U. S. A.* **2014**, *111* (2), 611−616.

(7) Marcus, R. A.; Sutin, N. Electron Transfers in Chemistry and Biology. *Biochimica et Biophysica Acta (BBA) - Reviews on Bioenergetics* **1985**, *811* (3), 265−322.

(8) Matsuura, Y. Coherent Spin Transport in a Multi-Heme Protein Molecule. *Chem. Phys.* **2022**, *558* (March), 111510.

(9) Eshel, Y.; Peskin, U.; Amdursky, N. Coherence-Assisted Electron Diffusion across the Multi-Heme Protein-Based Bacterial Nanowire. *Nanotechnology* **2020**, *31* (31), 314002.

(10) Ru, X.; Zhang, P.; Beratan, D. N. Assessing Possible Mechanisms of Micrometer-Scale Electron Transfer in Heme-Free Geobacter Sulfurreducens Pili. *J. Phys. Chem. B* **2019**, *123* (24), 5035−5047.

(11) Engel, G. S.; Calhoun, T. R.; Read, E. L.; Ahn, T. K.; Mančal, T.; Cheng, Y. C.; Blankenship, R. E.; Fleming, G. R. Evidence for Wavelike Energy Transfer through Quantum Coherence in Photosynthetic Systems. *Nature* **2007**, *446* (7137), 782−786.

(12) Diercksen, G.; McWeeny, R. Self-Consistent Perturbation Theory. I. General Formulation and Some Applications. *J. Chem. Phys.* **1966**, *44* (9), 3554−3560.

(13) Koopmans, T. Über Die Zuordnung von Wellenfunktionen Und Eigenwerten Zu Den Einzelnen Elektronen Eines Atoms. *Physica* **1934**, *1* (1−6), 104−113.

(14) Roothaan, C. C. J. Self-Consistent Field Theory for Open Shells of Electronic Systems. *Rev. Mod. Phys.* **1960**, *32* (2), 179−185.

(15) Hillier, I. H.; Saunders, V. R. A NewSCF Procedure and Its Applications Toab Initio Calculations of the States of the Fluorosulphate Radical. *Int. J. Quantum Chem.* **1970**, *4* (5), 503−518.

(16) McWeeny, R.; Diercksen, G. Self-Consistent Perturbation Theory. II. Extension to Open Shells. *J. Chem. Phys.* **1968**, *49* (11), 4852−4856.

(17) Tsuchimochi, T.; Scuseria, G. E. Communication: ROHF Theory Made Simple. *J. Chem. Phys.* **2010**, *133* (14), 141102.

(18) Huheey, J. E.; Keiter, E. A.; Keiter, R. L. *Inorganic Chemistry: Principles of Structure and Reactivity*, 4th ed.; Harper Collins: New York, USA, 1993.

(19) Niu, J.; Dong, S. An Integrated Calcium Fluoride Crystal Ir Thin-Layer Cell and Its Application to Identification of Electrochemical Reduction Product of Bilirubin. *Electrochim. Acta* **1995**, *40* (7), 823−828.

(20) Smith, D. M. A.; Dupuis, M.; Vorpagel, E. R.; Straatsma, T. P. Characterization of Electronic Structure and Properties of a Bis(Histidine) Heme Model Complex. *J. Am. Chem. Soc.* **2003**, *125* (9), 2711−2717.

(21) Livernois, W.; Anantram, M. P. Quantum Transport in Conductive Bacterial Nanowires. *2021 IEEE 16th Nanotechnology Materials and Devices Conference, NMDC 2021*; IEEE, 2021; pp 1−5, DOI: 10.1109/NMDC50713.2021.9677490.

(22) Qi, J.; Edirisinghe, N.; Rabbani, M. G.; Anantram, M. P. Unified Model for Conductance through DNA with the Landauer-Büttiker Formalism. *Phys. Rev. B* **2013**, *87* (8), 085404.

(23) Mohammad, H.; Demir, B.; Akin, C.; Luan, B.; Hihath, J.; Oren, E. E.; Anantram, M. P. Role of Intercalation in the Electrical Properties of Nucleic Acids for Use in Molecular Electronics. *Nanoscale Horiz* **2021**, *6* (8), 651−660.

(24) Grabert, H.; Devoret, M. H.; Kastner, M. Single Charge Tunneling, Coulomb Blockade Phenomena in Nanostructures. *Phys. Today* **1993**, *46* (4), 62−63.

(25) Xiong, Z. H.; Wu, D.; Valy Vardeny, Z.; Shi, J. Giant Magnetoresistance in Organic Spin-Valves. *Nature* **2004**, *427* (6977), 821−824.

(26) Frisch, M. J.; Trucks, G. W.; Schlegel, H. B.; Scuseria, G. E.; Robb, M. A.; Cheeseman, J. R.; Scalmani, G.; Barone, V.; Petersson, G. A.; Nakatsuji, H.; Li, X.; Caricato, M.; Marenich, A.; Bloino, J.; Janesko, B. G.; Gomperts, R.; Mennucci, B.; Hratchian, H. P.; Ortiz, J.; Izmaylov, A. F.; Sonnenberg, J. L.; Williams-Young, D.; Ding, F.; Lipparini, F.; Egidi, F.; Goings, J.; Peng, B.; Petrone, A.; Henderson, T.; Ranasinghe, D.; Zakrzewski, V. G.; Gao, J.; Rega, N.; Zheng, G.;

Liang, W.; Hada, M.; Ehara, M.; Toyota, K.; Fukuda, R.; Hasegawa, J.; Ishida, M.; Nakajima, T.; Honda, Y.; Kitao, O.; Nakai, H.; Vreven, T.; Throssell, K.; Montgomery, J. A., Jr.; Peralta, J. E.; Ogliaro, F.; Bearpark, M. J.; Heyd, J. J.; Brothers, E. N.; Kudin, K. N.; Staroverov, V. N.; Keith, T. A.; Kobayashi, R.; Normand, J.; Raghavachari, K.; Rendell, A. P.; Burant, J. C.; Iyengar, S. S.; Tomasi, J.; Cossi, M.; Millam, J. M.; Klene, M.; Adamo, C.; Cammi, R.; Ochterski, J. W.; Martin, R. L.; Morokuma, K.; Farkas, O.; Foresman, J. B.; Fox, D. J. *Gaussian 16*, revision C.01; Gaussian Inc.: Wallingford, CT, 2016.

(27) Leitão, E. F. v.; Ventura, E.; de Santana, O. L.; do Monte, S. A. Electronic Properties of the Low-Lying Spin States of Dimethylnitrosamine Coordinated to Fe(III) Heme Models: An Ab Initio Study. *Int. J. Quantum Chem.* **2014**, *114* (8), 508−520.

(28) Hay, P. J.; Wadt, W. R. Ab Initio Effective Core Potentials for Molecular Calculations. Potentials for K to Au Including the Outermost Core Orbitals. *J. Chem. Phys.* **1985**, *82* (1), 299−310.

(29) Petersson, G. A.; Al-Laham, M. A. A Complete Basis Set Model Chemistry. II. Open-shell Systems and the Total Energies of the First-row Atoms. *J. Chem. Phys.* **1991**, *94* (9), 6081−6090.

(30) Tomasi, J.; Mennucci, B.; Cammi, R. Quantum Mechanical Continuum Solvation Models. *Chem. Rev.* **2005**, *105* (8), 2999−3094.

(31) Verzijl, C. J. O.; Seldenthuis, J. S.; Thijssen, J. M. Applicability of the Wide-Band Limit in DFT-Based Molecular Transport Calculations. *J. Chem. Phys.* **2013**, *138* (9), 094102.

(32) Wilhelm, J.; Walz, M.; Evers, F. Ab Initio Spin-Flip Conductance of Hydrogenated Graphene Nanoribbons: Spin-Orbit Interaction and Scattering with Local Impurity Spins. *Phys. Rev. B* **2015**, *92* (1), 014405.

Recommended by ACS

Ultrafast and Electrically Tunable Rabi Frequency in a Germanium Hut Wire Hole Spin Qubit

He Liu, Guo-Ping Guo, *et al.*

APRIL 26, 2023
NANO LETTERS

READ

Localization and Directionality of Surface Transport in Bi_2Te_3 Ordered 3D Nanonetworks

Alejandra Ruiz-Clavijo, Marisol Martín-González, *et al.*

JULY 06, 2023
ACS NANO

READ

Evolution of 4π-Periodic Supercurrent in the Presence of an In-Plane Magnetic Field

Bassel Heiba Elfeky, Javad Shabani, *et al.*

FEBRUARY 17, 2023
ACS NANO

READ

Manipulation of the Magnetic State of a Porphyrin-Based Molecule on Gold: From Kondo to Quantum Nanomagnet via the Charge Fluctuation Regime

Yingzheng Gao, Stéphane Pons, *et al.*

MAY 10, 2023
ACS NANO

READ

Get More Suggestions >

https://doi.org/10.1021/acsnano.2c12027
ACS Nano 2023, 17, 9059−9068